Theoretical Analysis of a Wall-Mounted Broadband Antenna for Source Stirred Reverberation Chambers

# Theoretical Analysis of a Wall-Mounted Broadband Antenna for Source Stirred Reverberation Chambers

A. De Leo, P. Russo, V. Mariani Primiani
Department of Information Engineering
Università Politecnica delle Marche
Ancona, Italy
a.deleo@univpm.it

*Abstract* — **This paper is based on the analytical formulation of a method for predicting the electromagnetic field radiated by a wire antenna placed in a reverberation chamber. The antenna is discretized by a series of oblique segments. After verifying this assumption using full-wave numerical simulations, the proposed model is applied to a broadband antenna designed for a multiple antenna source stirred reverberation standard. The model can be used to analyze the performance of the chamber with respect to a number of indicators. This analysis has been extended to the entire frequency range in which the chamber has been experimentally characterized**

***Keywords-component: reverberation chamber; source stirring; statistical analysis;***

## I. INTRODUCTION

Reverberation Chambers (RCs) are metallic cavities commonly used for EMC testing [1] in which the electromagnetic field is properly stirred to obtain uniformity, anisotropy, and polarization freedom properties within the working volume.

There are many stirring actions [2], which are mainly divided into two families: mechanical stirring techniques, which are based on the change of boundary conditions by the movement of metal elements [3-5], and source stirring techniques [6], in which the stirring action is obtained by varying the coupling between the modes of the chamber and the sources.

One of the techniques belonging to the second family is called Multiple Antenna Source Stirring because it is based on an array of antennas placed on the walls of the chamber and fed in sequence to stir the electromagnetic field. This technique was originally proposed [7] and experimentally validated [8] using monopole antennas and its performances have been successfully compared with the mechanical stirring technique, both numerically [9] and experimentally [10].

The main limitation of using monopoles is that they are inherently narrowband antennas. For this reason, in this paper, we analyze the possibility of increasing the bandwidth of the method using a broadband antenna. First, a broadband antenna in free space was designed numerically and tested using full-wave analysis. Second, an analytical approach has been developed to determine the behavior of this antenna in a rectangular cavity. In this way, the main indicators describing the performance of the antenna in a RC can be predicted without the need of using numerical models, which are usually computationally expensive.

## II. NUMERICAL MODEL OF THE ANTENNA

The antenna chosen is the helical antenna proposed in [11]. This antenna can be analyzed analytically only simplifying its geometry with a series of straight elements. So it is necessary to test the assumptions that the behavior of the simplified antenna is the same as the original one.

To check this assumption, we used the Time Domain Solver from CST Microwave Studio. The antenna is simplified using 31, 51 and 75 segments, and the reflection coefficient of the original antenna is compared with the ones of the simplified versions.

Figure 1 shows the numerical model of the helical antenna (top) and its approximation with 31 segments (bottom).

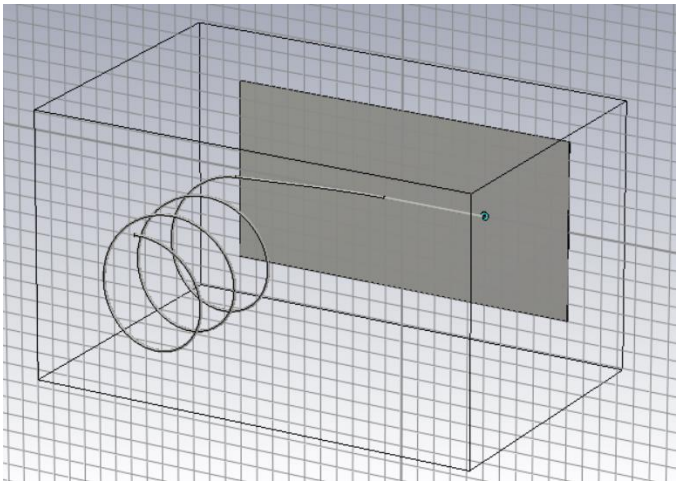

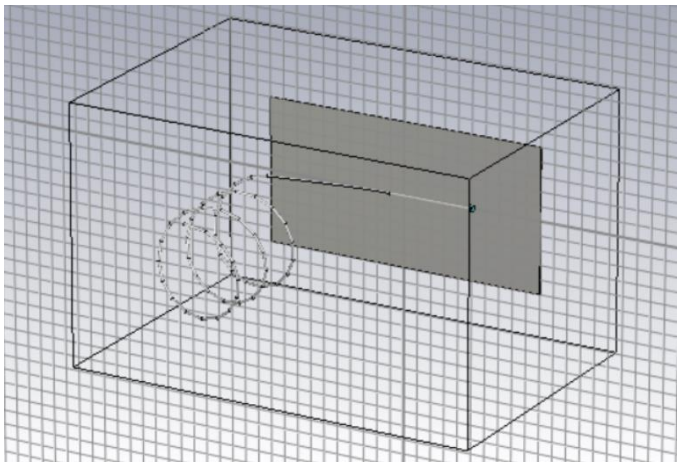

Fig.1. Geometry of the antenna using an analytical representation of the helix (top) and an approximation obtained using 31 segments (bottom).

The helix has a pitch of 42 mm (pitch angle 12°), a radius of 35 mm, and it is composed by 3 turns.

Figure 2 shows the S11 parameters of the 4 antennas. The results suggest that there is not much difference in terms of reflection parameter between the analytical representation of the helix and the representation obtained using segments.

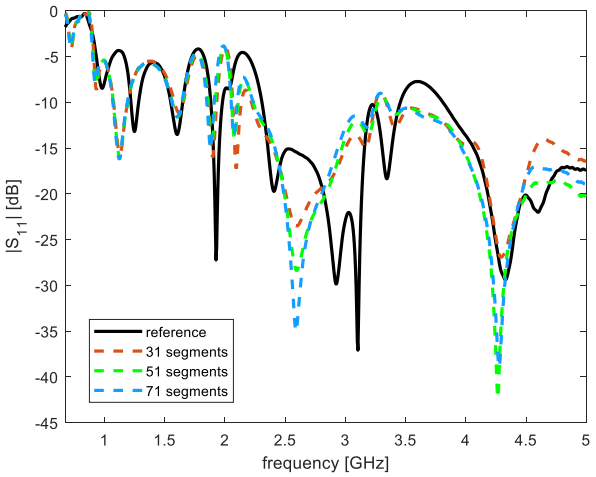


Fig.2. Reflection parameter simulated for the analytical model (reference values) and the approximation using 31 (red), 51 (green) and 71(blue) segments.

In particular, the simplified models of the antenna give almost the same coefficients so, in order to represent the antenna, it is sufficient to use the one with the smallest number of segments.

## III. Analytical Model of The Antenna in RC

In this section the analytical model for the evaluation of the field radiated by the helix inside a RC is presented. The antenna is represented as a superposition of linear current elements, as determined in the previous section.

The analytical model, that predicts the electromagnetic field radiated by the helix into a RC, is based on superposition technique and on the analytical equations that describe a generic oblique electric dipole as source for the cavity mode excitation. Let's consider a dipole, directed from $P_0(x_0,y_0,z_0)$ to $P_1(x_1,y_1,z_1)$, fed by a current $I_0$ and placed into a rectangular cavity having dimensions (a × b × c), as shown in Figure 3.

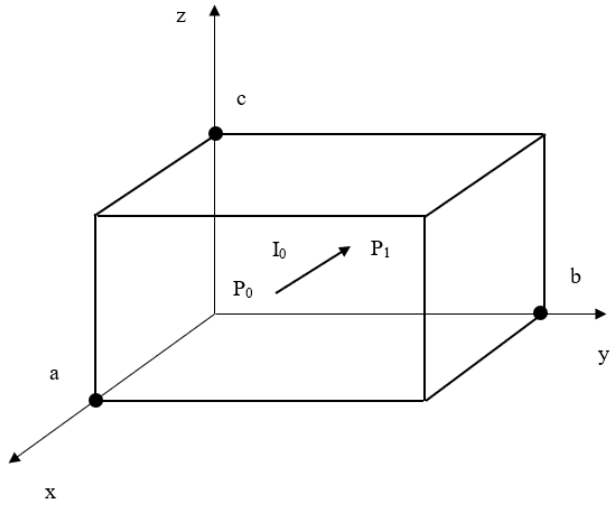


Fig.3. An oblique segment, fed by a current $I_0$, placed in a rectangular cavity.

The electric field ($\bar{E}$ ) generated by this element can be written as (1) the sum of the irrotational component ($\bar{E}^{IRR}$) and the solenoidal ones ($\bar{E}^{TE}, \bar{E}^{TM}$).

$$\bar{E}\,(\bar{I}) = \bar{E}^{IRR}(\bar{I}) + \bar{E}^{TE}(\bar{I}) + \bar{E}^{TM}(\bar{I}) \qquad (1)$$

Each term of this equation can be calculated analytically thanks to the modal expansion of the electromagnetic field into a rectangular cavity

$$\bar{E}^{IRR}(\bar{I}) = -\frac{1}{j\omega\varepsilon}\sum_{mnp}\left(\int_V \bar{J}\cdot\overline{f_m}dv\right)\overline{f_m} =$$
$$-\frac{I_0}{j\omega\varepsilon}\frac{8}{abc}\sum_{mnp}\frac{1}{k_{mnp}^2}\left\{\frac{x_1-x_0}{R}k_x Int_1 + \frac{y_1-y_0}{R}k_y Int_2 + \right.$$
$$\left.\frac{z_1-z_0}{R}k_z Int_3\right\}\begin{bmatrix} k_x cos(k_x x)sin(k_y y)sin(k_z z)\hat{x} \\ k_y sin(k_x x)cos(k_y y)sin(k_z z)\hat{y} \\ k_z sin(k_x x)sin(k_y y)cos(k_z z)\hat{z}\end{bmatrix}, \qquad (2)$$

$$\bar{E}^{TE}(\bar{I}) = -j\omega\mu\sum_{mnp}\frac{\int_V \bar{J}\cdot\bar{e}_m^{TE}dv}{k_{mnp}^2-\beta_{TE}^2}\bar{e}_m^{TE} =$$
$$-j\omega\mu I_0\frac{8}{abc}\sum_{mnp}\frac{1}{(k_x^2+k_x^2)}\frac{I_0}{k_{mnp}^2-\beta_{TE}^2}\left\{-\frac{x_1-x_0}{R}k_y Int_1 + \right.$$
$$\left.\frac{y_1-y_0}{R}k_x Int_2\right\}\cdot\begin{bmatrix} -k_y cos(k_x x)sin(k_y y)sin(k_z z)\hat{x} \\ +\,k_x sin(k_x x)cos(k_y y)sin(k_z z)\hat{y}\end{bmatrix}, \qquad (3)$$

$$\bar{E}^{TM}(\bar{I}) = -j\omega\mu \sum_{mnp} \frac{\int_V \bar{J}\cdot \bar{e}_m^{TM} dv}{k_{mnp}^2 - \beta_{TM}^2} \bar{e}_m^{TM}$$
$$= -j\omega\mu I_0 \frac{8}{abc} \sum_{mnp} \frac{1}{k_{mnp}^2} \frac{1}{k_{mnp}^2 - \beta_{TM}^2} \left\{ -\frac{x_1 - x_0}{R} k_x k_z Int_1 \right.$$
$$\left. - \frac{y_1 - y_0}{R} k_y k_z Int_2 + \frac{z_1 - z_0}{R} (k_x^2 + k_x^2) \cdot Int_3 \right\}$$
$$\begin{bmatrix} -\frac{k_x k_z}{k_e^2} cos(k_x x) sin(k_y y) sin(k_z z)\hat{x} \\ -\frac{k_y k_z}{k_e^2} sin(k_x x) cos(k_y y) sin(k_z z)\hat{y} \\ +sin(k_x x) sin(k_y y) cos(k_z z)\hat{z} \end{bmatrix}, \quad (4)$$

where $\bar{f}_{m,n,p}$ and $\bar{e}_{m,n,p}^{TE,TM}$ are irrotational and TE, TM divergenceless electric eigenvectors respectively, and

$$R = \sqrt{(x_1 - x_0)^2 + (y_1 - y_0)^2 + (z_1 - z_0)^2} \quad (5)$$

$$\beta_{TE,TM}^2 = \beta^2 \left[ 1 - (-1 + j) \frac{\omega_{n,m,p}}{\omega Q_{m,n,p}^{TE,TM}} \right], \quad (6)$$

where $k_{m,n,p}$ , $Q_{m,n,p}^{TE,TM}$ and $\omega_{n,m,p}$ are the corresponding eigenvalues, quality factors, and resonant angular frequencies, respectively, and $\beta^2 = \omega^2\mu\epsilon$.

$Q_{m,n,p}^{TE,TM}$ is the quality factor of each mode, and it is calculated considering an equivalent wall conductivity value retrieved from real chamber measurements [8].

Expressions of $Int_3$, $Int_3$ and $Int_3$ are reported in Appendix for sake of readability.

## IV. Simulated Scenario and Results

The scenario simulated with the analytical model described in the previous section is a rectangular cavity with dimensions 800 mm × 900 mm × 1000 mm (Fig. 3). In each side of the chamber there are 20 positions where the antenna is inserted to feed the chamber. These positions are corresponding to holes made on the walls of the RC available in our labs.

The numerical simulations of the 31-segments antenna return a complex value of the current in each segments. All these oblique current elements are inserted in the model of section III to compute the field inside the chamber using the superposition.

Thanks to the model it was possible to compute some indicators useful to estimate the performances of the RC:

- the field uniformity;
- the field anisotropy;
- the field inhomogeneity;
- the field statistics.

### A. Field Uniformity

The field uniformity was calculated according to the standard [1]. The eight vertex of the working volume was chosen at a distance of 150 mm from the walls of the RC.

Figure 4 shows that the predictions of the proposed analytical models are in good accordance with the results of the full-wave numerical simulations [11]. In fact, according to both numerical and analytical analysis, the uniformity of the electric field meets the standard requirements for frequencies greater than 2 GHz.

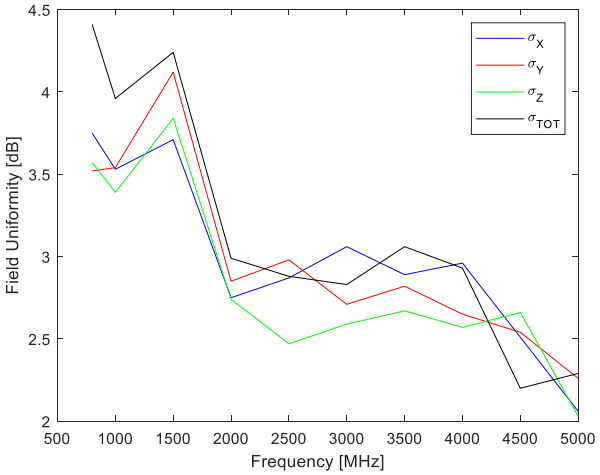


Fig.4. Electric field uniformity, computed according to the standard [1].

### B. Field Anisotropy

Figure 5 shows the behavior of field anisotropy computed in the central point of the RC, according to the standard [1] and research [13].

Also for this indicator, the predictions of the analytical model agree with the result of the numerical simulations [11]. Above 2 GHz, the anisotropy shows a behavior that lies between average and good thresholds, considering the number of independent field configurations.

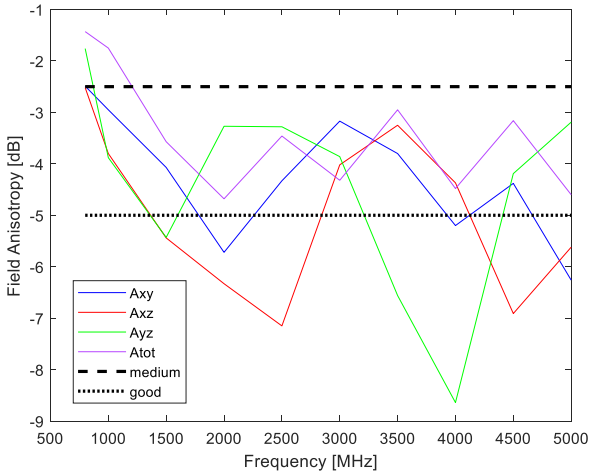


Fig.5. Electric field anisotropy computed according to the standard [1]. Medium and good threshold are represented by black lines.

### C. Field Inhomogeneity

In this subsection the electric field inhomogeneity was considered; in particular this parameter was calculated between

one of the eight corners of the working volume, having coordinates $P_1$(150 mm, 150 mm, 150 mm) and the central point $P_0$(400 mm, 450 mm, 500 mm).

The field inhomogeneity was defined as (7), according to [14]:

$$I_{\alpha i}(\bar{r}) = \frac{\left|\frac{E^{+}_{\alpha i}(\bar{r})}{\sigma^{+}_{\alpha i}}\right|^2 - \left|\frac{E^{-}_{\alpha i}(\bar{r})}{\sigma^{-}_{\alpha i}}\right|^2}{\left|\frac{E^{+}_{\alpha i}(\bar{r})}{\sigma^{+}_{\alpha i}}\right|^2 + \left|\frac{E^{-}_{\alpha i}(\bar{r})}{\sigma^{-}_{\alpha i}}\right|^2}, \quad (7)$$

where $\alpha = x, y, z$, $\bar{r} = \overline{P_1 - P_0}$ and $\sigma^{\pm}_{\alpha i}$ is the standard deviation of the $E^{\pm}_{\alpha i}(\bar{r})$ component.

Figure 6 shows the frequency behavior of this parameter; it can be appreciated a value below -3 dB in the whole considered frequency range.

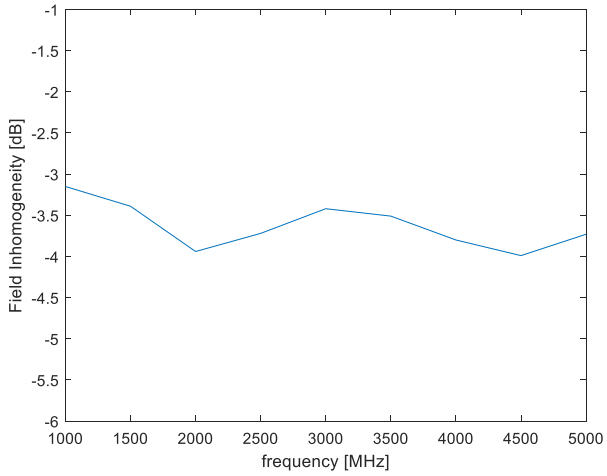


Fig.6. Electric field inhomogeneity

### D. Electric Field Statistics

The ideal electric field distribution in an ideally stirred RC is a Rayleigh distribution. For this reason, the electric field distribution simulated by the proposed analytical model was compared with the CHI6DOF using the MATLAB function *[h, p] = kstest2(x1, x2).* It provides a test decision for the null hypothesis that the data in vectors x1 and x2 are from the same continuous distribution using the Kolmogorov-Smirnov two-sample test. The result h is 1 if the test rejects the null hypothesis at a 5% significance level, and 0 otherwise. The kstest2 function also yields the asymptotic p-value p, shown in Fig. 7 as the frequency-dependent behavior of this parameter. As expected, the RC is significantly overdriven at higher frequencies and the statistics of the simulated field tend towards the ideal distribution.

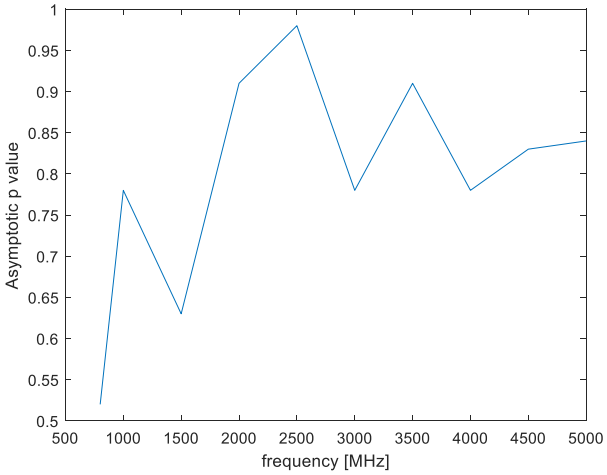


Fig.7. Asymptotic p-value returned by kstest2 function of the electric field.

## V. CONCLUSIONS

In this paper, the performances of a broadband helical antenna have been investigated by an analytical model of the RC.

To that purpose, the helical structure has been discretized into a sufficient number of oblique elements that can be represented using the proposed analytical model. After validating the assumptions that the discretized antenna is almost equivalent to the original antenna, it has been used inside the analytical model with suitable current distribution, to obtain a set of indicators that can be used to estimate the performances of the RC. The results highlighted the sought broadband behavior of the RC fed by the considered antenna.

Future work will address the extension of the proposed model to predict the impedance of the antenna and thus obtain the analytical distribution of the current along with the wire antenna.

## REFERENCES


[1] Reverberation Chamber Test Methods, International Electrotechnical Commission (IEC), Std. 61 000-4-21, 2011.

[2] R. Serra et al., “Reverberation chambers a la carte: An overview of the different mode-stirring techniques”, in IEEE Electromagnetic Compatibility Magazine, vol. 6, no. 1, pp. 63-78, First Quarter 2017

[3] P. Corona, G. Latmiral, E. Paolini, L. Piccioli, "Use of reverberating enclosure for measurement of radiated power in the microwave range", IEEE Trans. on EMC., vol. 18, no. 2, pp. 54-59, May 1976. DOI: 10.1109/TEMC.1976.303466

[4] F. Leferink, J. C. Boudenot, W. Van Etten, “Experimental results obtained in the vibrating intrinsic reverberation chamber,” IEEE Int. Symp. Electromagnetic Compatibility, 639–644, Washington, 21-25 Aug. 2000. DOI: 10.1109/ISEMC.2000.874695

[5] D. Barakos and R. Serra, "Performance characterization of the oscillating wall stirrer," 2017 International Symposium on Electromagnetic Compatibility - EMC EUROPE, Angers, 2017, pp. 1-4. DOI: 10.1109/EMCEurope.2017.8094726

[6] Y. Huang and D. J. Edwards, “A novel reverberating chamber: source-stirred chamber,” *IEE 8th International Conference on Electromagnetic Compatibility*, pp.120-124, Edinburgh, UK, September 1992

[7] A. De Leo, V. M. Primiani, P. Russo and G. Cerri, "Low-Frequency Theoretical Analysis of a Source-Stirred Reverberation Chamber," *IEEE Transaction on Electromagnetic Compatibility* vol. 59, no. 2, pp. 315-324, April 2017. DOI: 10.1109/TEMC.2016.2613402

[8] A. D. Leo, G. Cerri, P. Russo and V. M. Primiani, "Experimental Validation of an Analytical Model for the Design of Source-Stirred Chambers," in IEEE Transactions on Electromagnetic Compatibility, vol. 60, no. 2, pp. 540-543, April 2018. DOI: 10.1109/TEMC.2017.2723804

[9] A. De Leo, V. M. Primiani, P. Russo and G. Cerri, "Numerical analysis of a reverberation chamber: Comparison between mechanical and source stirring techniques," 2017 International Symposium on Electromagnetic Compatibility - EMC EUROPE, Angers, 2017, pp. 1-6, doi: 10.1109/EMCEurope.2017.8094648.

[10] A. De Leo, G. Cerri, P. Russo and V. Mariani Primiani, "Experimental Comparison Between Source Stirring and Mechanical Stirring in a Reverberation Chamber by Analyzing the Antenna Transmission Coefficient," 2018 International Symposium on Electromagnetic Compatibility (EMC EUROPE), Amsterdam, 2018, pp. 677-682, doi: 10.1109/EMCEurope.2018.8485091

[11] A. De Leo, G. Cerri, P. Russo and V. M. Primiani, "Design of a Broadband Antenna for a Reverberation Chamber with Multiple Antenna Source Stirring," 2021 IEEE International Joint EMC/SI/PI and EMC Europe Symposium, 2021, pp. 350-354, doi: 10.1109/EMC/SI/PI/EMCEurope52599.2021.9559246.

[12] 3ds: 'CST Microwave Studio' [online] https://www.3ds.com/products services/simulia/products/cst studio suite, accessed: January 2022

[13] L. R. Arnaut, R. Serra and P. D. West, "Validating reverberation chamber performance based on assessment of field anisotropy," 2016 International Symposium on Electromagnetic Compatibility - EMC EUROPE, 2016, pp. 205-210, doi: 10.1109/EMCEurope.2016.7739171.

[14] L. R. Arnaut, "Field anisotropy, field inhomogeneity and polarization bias in imperfect reverberation chambers," Nat. Phys. Lab., Teddington, U.K., Tech. Rep. R981120, pp. 1–65, Nov. 1998.

## APPENDIX

In this section there are reported the expressions of $Int_1$, $Int_2$ and $Int_3$, used in formulas (2) (3) and (4).

$$Int_1 = \frac{S(\theta,\varphi)}{4}\left\{\frac{sin(k_x x_1 + k_y y_1 - k_z z_1) - sin(k_x x_0 + k_y y_0 - k_z z_0)}{(k_x + k_y m_y - k_z m_z)} + \frac{sin(-k_x x_1 + k_y y_1 - k_z z_1) - sin(-k_x x_0 + k_y y_0 - k_z z_0)}{(-k_x + k_y m_y - k_z m_z)} - \right.$$
$$- \frac{sin(k_x x_1 + k_y y_1 + k_z z_1) - sin(k_x x_0 + k_y y_0 + k_z z_0)}{(k_x + k_y m_y + k_z m_z)} -$$
$$\left. - \frac{\sin(-k_x x_1 + k_y y_1 + k_z z_1) - \sin(-k_x x_0 + k_y y_0 + k_z z_0)}{(-k_x + k_y m_y + k_z m_z)}\right\}, \quad (A.1)$$

$$Int_2 = \frac{S(\theta,\varphi)}{4}\left\{\frac{sin(k_x x_1 + k_y y_1 - k_z z_1) - sin(k_x x_0 + k_y y_0 - k_z z_0)}{(k_x + k_y m_y - k_z m_z)} + \frac{sin(k_x x_1 - k_y y_1 - k_z z_1) - sin(k_x x_0 - k_y y_0 - k_z z_0)}{(k_x - k_y m_y - k_z m_z)} - \right.$$
$$- \frac{sin(k_x x_1 + k_y y_1 + k_z z_1) - sin(k_x x_0 + k_y y_0 + k_z z_0)}{(k_x + k_y m_y + k_z m_z)} -$$
$$\left. - \frac{\sin(k_x x_1 - k_y y_1 + k_z z_1) - \sin(k_x x_0 - k_y y_0 + k_z z_0)}{(k_x - k_y m_y + k_z m_z)}\right\}, \quad (A.2)$$

$$Int_3 = \frac{S(\theta,\varphi)}{4}\left\{\frac{sin(k_x x_1 - k_y y_1 + k_z z_1) - sin(k_x x_0 - k_y y_0 + k_z z_0)}{(k_x - k_y m_y + k_z m_z)} + \frac{sin(k_x x_1 - k_y y_1 - k_z z_1) - sin(k_x x_0 - k_y y_0 - k_z z_0)}{(k_x - k_y m_y - k_z m_z)} - \right.$$
$$- \frac{sin(k_x x_1 + k_y y_1 + k_z z_1) - sin(k_x x_0 + k_y y_0 + k_z z_0)}{(k_x + k_y m_y + k_z m_z)} -$$
$$\left. - \frac{\sin(k_x x_1 + k_y y_1 - k_z z_1) - \sin(k_x x_0 + k_y y_0 - k_z z_0)}{(k_x + k_y m_y - k_z m_z)}\right\}, \quad (A.3)$$

where

$$S(\theta,\varphi) = cos\varphi sin\theta + m_y sin\varphi sin\theta + m_z cos\theta\,, \quad (A.4)$$

being

$$cos\varphi = \frac{(x_1 - x_0)}{\sqrt{(x_1 - x_0)^2 + (y_1 - y_0)^2}}\,, \quad (A.5)$$

$$sin\varphi = \frac{(y_1 - y_0)}{\sqrt{(x_1 - x_0)^2 + (y_1 - y_0)^2}}\,, \quad (A.6)$$

$$sin\theta = \frac{\sqrt{(x_1 - x_0)^2 + (y_1 - y_0)^2}}{\sqrt{(x_1 - x_0)^2 + (y_1 - y_0)^2 + (z_1 - z_0)^2}}, \quad (A.7)$$

$$cos\theta = \frac{z_1 - z_0}{\sqrt{(x_1 - x_0)^2 + (y_1 - y_0)^2 + (z_1 - z_0)^2}}, \quad (A.8)$$

and

$$m_y = \frac{y_1 - y_0}{x_1 - x_0}, \quad (A.9)$$

$$m_z = \frac{z_1 - z_0}{x_1 - x_0}. \quad (A.10)$$